A Phase Field Method with Adaptive Mesh Refinement for Numerical Simulation of 3D Wetting Processes with OpenFOAM®

Xuan Cai[1], Holger Marschall[2], Martin Wörner[1] and Olaf Deutschmann[1]

[1] Karlsruhe Institute of Technology, Institute of Catalysis Research and Technology, 76021 Karlsruhe, Germany

[2] Technische Universität Darmstadt, Center of Smart Interfaces, 64287 Darmstadt, Germany

Abstract

In this paper, we use a phase field method coupled with the Navier-Stokes equations for numerical investigation of wetting phenomena. Simulations on capillary rise and droplet wetting on a flat substrate with fixed grids produce steady computational results in good agreement with analytical solutions and experimental data in the literature. As key element to achieve CPU-time efficient simulations, we present the first 3D finite-volume based phase-field simulations for wetting phenomena with adaptive mesh refinement around interface, to the best of our knowledge. Results for the droplet motion on an inclined plane indicate that the droplet speed depends critically on the mobility. Since in our phase-field method, the mobility (respectively the corresponding Peclet number) is rather a numerical than a physically measurable parameter, we conclude that the method is not yet predictive for droplet sliding on inclined surface.

KEY WORDS

Computational Multiphase Fluid Dynamics, Droplet Spreading, Moving Contact Lines

1. Introduction

The wetting of liquid on solid surface is a crucial process in many applications in chemical industry, such as coating, painting, and reacting two-phase flows in chemical sponge reactors, for instance. The technological improvement of these processes requires precise knowledge of wetting dynamics. To gain these insights, CFD can be a valuable tool. For reliable CFD simulations, it is vital to model accurately the motion of the contact line where the two-phase flow is in contact with the solid surface. In this context, conventional sharp-interface hydrodynamic models suffer from a paradox between the moving contact line and no-slip boundary condition at the solid wall [1]. To resolve this problem, various methods have been proposed (e.g., the precursor film model [2] and the slip model [3]).

Among the various methods for interfacial simulations of two-phase flows, the phase field method is probably the most promising approach for handling moving contact lines. It is a diffuse interface method that treats the interface between two immiscible fluids as a transition region of small but finite width, endowed with surface tension [4]. Based on fluid free energy instead of force, the method can be traced to van der Waals a century ago [5]. The phase field method has become popular just in recent years as a numerical technique for simulating two-phase flows with a wide range of hydrodynamic and interfacial phenomena [6]. In our study, the most significant feature of this method is that it allows motion of the contact line in combination with a no-slip boundary condition at a solid wall via a diffusive mechanism induced by a chemical potential gradient [7].

In this paper, we study wetting processes numerically, with the phase field method we have developed in OpenFOAM®. In Section 2, we present the mathematical formulation of the numerical method. Section 3 presents the 2D static-mesh simulations on capillary rise and droplet wetting, and demonstrates the method's capability with adaptive mesh refinement of 3D simulations of droplet wetting on flat/inclined substrates. In Section 4 we present the conclusions and outlook.

2. Mathematical formulation

2.1 The phase field method

For a two-phase flow of incompressible, viscous and isothermal fluids, we introduce an order parameter (C) to characterize the two different phases. C is defined as the difference in volumetric phase fractions of phase A/B, i.e. $C = \alpha_A - \alpha_B$. Thus, C takes distinct values $C_A = 1$ and $C_B = -1$ for bulk phase A/B and varies rapidly but smoothly in a thin layer which represents the diffuse interface. The interface dynamics is governed by an evolution equation for C, namely the Cahn-Hilliard equation that reads in non-dimensional form:

$$\frac{\partial C}{\partial t} + (\mathbf{u}\cdot\nabla)C = \frac{1}{Pe_\kappa}\nabla^2\phi\,, \tag{1}$$

where

$$\phi = C^3 - C - Cn^2\nabla^2 C \tag{2}$$

is the chemical potential.

The term on the right-hand-side of Eq. (1) provides a diffusive mechanism for motion of the contact line at a no-slip wall. Based on the wall free energy formulation at local equilibrium, one can derive the following boundary condition to account for the wettability of the solid substrate:

$$\hat{\mathbf{n}}_s\cdot\nabla C = -\frac{2\sqrt{2}\cos\theta_e}{3Cn}(0.75C^2 - 0.75C)\,, \tag{3}$$

where θ_e is the equilibrium (static) contact angle.

2.2 Equations of fluid flow

The single-field Navier-Stokes equations can be expressed in the dimensionless form

$$\nabla\cdot\mathbf{u} = 0\,, \tag{4}$$

$$\rho(C)Re\left(\frac{\partial\mathbf{u}}{\partial t} + (\mathbf{u}\cdot\nabla)\mathbf{u}\right) = -\nabla p + \mu(C)\nabla^2\mathbf{u} + \mathbf{f}_{st} + \mathbf{f}_b\,, \tag{5}$$

where the surface tension and buoyance force are given by

$$\mathbf{f}_{st} = -\frac{1}{Ca\cdot Cn}C\nabla\phi(C)\,, \tag{6}$$

$$\mathbf{f}_b = -\frac{1}{2}\frac{Eo}{Ca}(C+1)\mathbf{e}_z \tag{7}$$

The non-dimensional density and viscosity of the mixture are

$$\rho(C) = \frac{1}{2}\left((C+1) - \frac{\rho_B}{\rho_A}(C-1)\right), \tag{8}$$

$$\mu(C) = \frac{1}{2}\left((C+1) - \frac{\mu_B}{\mu_A}(C-1)\right) \tag{9}$$

Here, $\rho_{A,B}$ and $\mu_{A,B}$ are the density and viscosity of phase A/B. In these equations, t, $\mathbf{u}$ and p denote time, velocity field and pressure. Physical dimensionless groups are the Reynolds number $Re = \rho_A L_{ref} U_{ref}/\mu_A$, the capillary number $Ca = (8/9)^{0.5}\mu_A U_{ref}/\sigma$, and the Eötvös number $Eo = (\rho_A - \rho_B)gL_{ref}^2/\sigma$, where σ and g are surface tension coefficient and gravitational acceleration. In addition, there are two phase-field method specific non-dimensional parameters: the mobility Peclet number $Pe_\kappa = (8/9)^{0.5}L_{ref}U_{ref}\varepsilon/\kappa\sigma$ and the Cahn number $Cn = \varepsilon/L$, where ε and κ denote the interfacial width and mobility. Pe_κ indicates the ratio between the convective and diffusive transports of the order parameter. It quantifies the diffusion process that governs the motion of the contact line. Cn specifies the interface thickness. In the non-dimensional system, the length scale is L_{ref}, the velocity scale U_{ref}, and the time scale L_{ref}/U_{ref}. Based on this normalization, we show all simulation results in non-dimensional form.

2.3 Numerical treatment

In our previous study [8], the phase field method was coupled with the Navier-Stokes equations and implemented in OpenFOAM®. The method was verified and validated by various test problems, and the influence of Pe_κ and Cn was investigated. Based on the outcome of the previous study, we choose here at least four mesh cells for resolving the interface layer; for the Cahn number we use $Cn = 0.01$. In the following simulations, all spatial derivatives are approximated by central differences and time integration is performed by a backward scheme. For further details about the implementation and numerical setups we refer to [8].

3. Results and discussion

3.1 2D static-mesh simulations

3.1.1 Capillary rise

In this test case, we reproduce the capillary rise phenomenon driven by wall adhesion force, between two parallel plates if the distance between them (w) is small enough. In the simulation, initially the vertical channel is filled with air and the water is in the container (Figure 1a). When the simulation starts, the wall adhesion force causes the water to creep up

along the wall, to meet the prescribed equilibrium contact angle (Figure 1b). Then a pressure jump arises across the curved interface, and drives the water to move upward further (Figure 1c). The water keeps rising until the capillary force is balanced by the gravity force (Figure 1d).

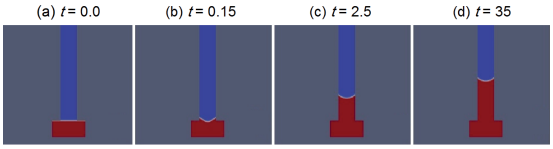

Figure 1: 2D simulation of capillary rise of water into the channel between two parallel plates. Equilibrium contact angle θ_e = 45°.

Based on the balance relation between the two forces, we can derive an analytical solution of the water final height

$$h = \frac{2\sigma\cos(\theta_e)}{\rho g w} \tag{10}$$

Steady simulation results for different values of the equilibrium contact angle θ_e agree well with the analytical solution (Figure 2).

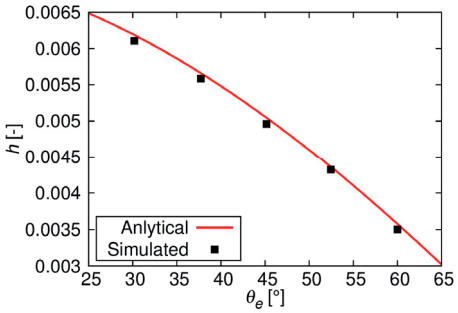

Figure 2: Final height of the water column.

3.1.2 Partial droplet wetting

3.1.2.1 Final droplet shape

We divide our study into two cases: one without gravity force ($Eo = 0$) and the other with gravity force ($Eo > 0$). In the case $Eo = 0$, the capillary effect is the only driving force for droplet wetting. We consider the following scenario: initially, a semi-circle droplet with initial radius R_0 and contact angle $\theta_0 = 90°$ is released on a flat surface (Figure 3a). If the equilibrium contact angle θ_e is different from θ_0, the contact line moves, and the droplet spreads to the equilibrium shape of a circular cap with θ_e [9] (Figure 3b).

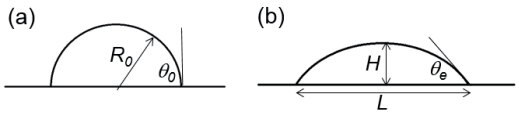

Figure 3: (a) initial shape of the droplet released on the surface. (b) equilibrium shape of the droplet

By conservation of droplet volume, the analytical spreading length L and the droplet height H at the equilibrium shape can be derived as:

$$L = 2R_0\sqrt{\frac{\pi}{2(\theta_e - \sin\theta_e\cos\theta_e)}}\sin\theta_e \tag{11}$$

$$H = R_0\sqrt{\frac{\pi}{2(\theta_e - \sin\theta_e\cos\theta_e)}}(1-\cos\theta_e) \tag{12}$$

We compare the analytical and simulated values of L and H in Figure 4. Good agreement is achieved in a wide range of surface wettability for both hydrophilic and hydrophobic situations (from $\theta_e = 45°$ to $\theta_e = 135°$). The best agreement is found when $\theta_e = 90°$, because the droplet remains stationary when $\theta_e = \theta_0$.

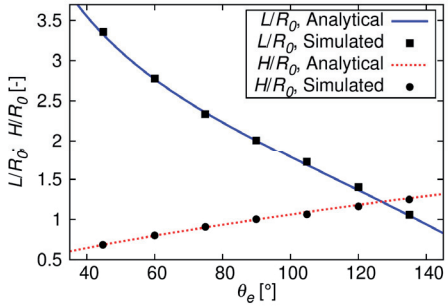

Figure 4: Analytical and simulated spreading length L and height H versus equilibrium contact angle θ_e.

In the case $Eo > 0$, the droplet is wetting the solid surface due to the combined effect of gravity and capillary forces: the gravity force tends to spread out the droplet further while the capillary force tends to maintain it as a circular cap. If $Eo << 1$, the capillary force is dominant. Thus, the droplet height (H_0) at the equilibrium shape is the same as in the case $Eo = 0$:

$$H_0 = R_0\sqrt{\frac{\pi}{2(\theta_e - \sin\theta_e\cos\theta_e)}}(1-\cos\theta_e) \tag{13}$$

For $Eo >> 1$, the gravity force dominates. The circular droplet forms to a puddle and its analytical height at the equilibrium shape (H_∞) is given by Eq. (14) [9].

$$H_\infty = \frac{2R_0}{\sqrt{Eo}} \sin\left(\frac{\theta_e}{2}\right) \quad (14)$$

Figure 5 shows equilibrium droplet shapes at $Eo = 0.1$, 1.0 and 10 from the simulations, with equilibrium contact angle $\theta_e = 60°$. It is evident that the droplet takes the shape of a circular cap at small Eo and of a puddle at large Eo. The droplet resembles an elongated circular cap at $Eo = 1.0$, where the capillary and gravity forces are of the same order of magnitude.

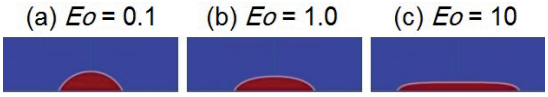

Figure 5: 2D simulated final droplet shapes at different Eötvös numbers; $\theta_e = 60°$.

In Figure 6, we plot the final droplet height H, normalized by H_0 from Eq. (13), as a function of Eo. The simulation results are in good agreement with the two asymptotic solutions given by Eq. (13) and Eq. (14), at small and large Eo respectively. As expected, we can observe a transition around $Eo = 1$.

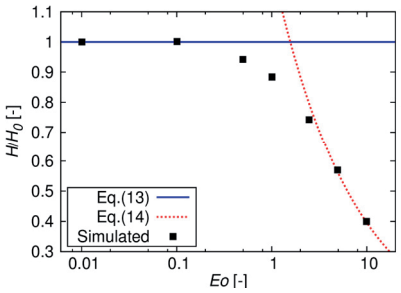

Figure 6: Normalized droplet height (H/H_0) as a function of Eo ($\theta_e = 60°$).

3.1.2.2 *Spreading dynamics*

To investigate the dynamic wetting process, we turn from planar to axisymmetric simulations and compare the time dependent results with experimental data of Zosel [10]. In the experiment, the instantaneous base radius of droplets composed of a PIB solution was recorded during their spreading process on a PTFE surface. All the droplets exhibit almost the same equilibrium contact angle ($\theta_e \approx 58° - 60°$). Their radii are in the range between 1.2–1.5 mm. Under such conditions, gravity and inertial forces are assumed negligible. Thus, the density difference between the droplet and ambient fluid can be neglected; the density ratio is assumed to 1 in the simulations.

In the experiment, the viscosity ratio, λ_μ, between the ambient fluid and droplet ranges from 10^{-3} to 10^{-6}. We set $\lambda_\mu = 0.05$ in our simulations to avoid numerical instability and to save computational effort. A sensitivity study on λ_μ shows that a further decrease does not affect the results significantly. The simulation results are compared with the experimental data in Figure 7, where good agreement is achieved, especially at the later spreading stage. It is observed that when Pe_κ is getting smaller, the spreading radius is changing faster, and the result is getting slightly closer to experimental data. This is reasonable since motion of moving contact line in phase field method is governed by diffusion. Thus, a stronger diffusion by setting a smaller Pe_κ leads to a faster spreading.

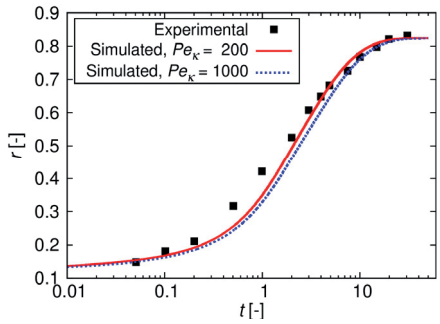

Figure 7: Temporal evolution of droplet's base radius; 2D axisymmetric simulations with $Re = 1.0$, $Ca = 0.94$, $Cn = 0.01$, $Eo = 0$, $\theta_0 = 170°$, $\theta_e = 58°$, $\lambda_\mu = 0.05$; Experimental data from Zosel [10].

3.2 *3D adaptive mesh simulations*

A key element to achieve high numerical accuracy with a moderate computational cost in 3D is the use of local adaptive mesh refinement (AMR), allowing to provide significantly higher mesh densities where it is most needed – at the interface. This is particularly important for diffuse interface simulation, since the interface must be thin enough to converge to sharp-interface limit yet adequately resolved for interfacial effects to be computed accurately [11]. In this section, we demonstrate the capabilities of our method with 3D AMR for interface region. The adaptive mesh refinement is handled by the class *dynamicRefineFvMesh* in the OpenFOAM® C++ library. Here we define the interface region where $-0.9 < C < 0.9$ [4]. In simulations, we set a two level mesh refinement for the interface region compared with the bulk region (see Figure 8). The mesh refinement is made adaptively at each time step.

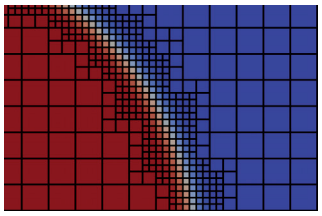

Figure 8: A hexahedral mesh with two level AMR for interface region.

3.2.1 Droplet wetting on flat substrate

Figure 9 depicts a 3D AMR simulation of droplet spreading on a flat substrate with equilibrium contact angle $\theta_e = 75°$. We neglect gravity so the spreading is driven by capillary force alone. We start with a spherical droplet with initial contact angle of $170°$ (Figure 9a). As time proceeds, the droplet is spreading out (Figure 9b and Figure 9c) and approaching to the final state with the prescribed equilibrium contact angle $\theta_e = 75°$ (Figure 9d).

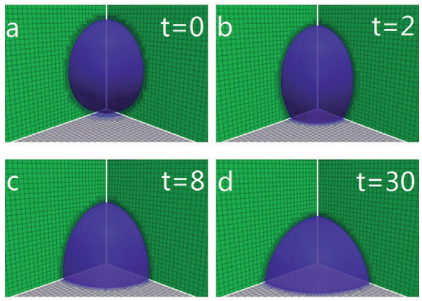

Figure 9: 3D AMR simulation of droplet spreading (one-quarter geometry) on a flat substrate from initial state (a) to equilibrium state (d). $\theta_0 = 170°$, $\theta_e = 75°$, $Re = 1.0$, $Ca = 0.94$, $Pe_\kappa = 1000$, $Cn = 0.01$, $Eo = 0$, $\lambda_\mu = 0.1$.

To validate the 3D AMR simulations, we compare their results against those from 2D static-mesh axisymmetric simulations with the same physical and numerical parameters and interface mesh resolutions. Figure 10 shows a close agreement, both for the case $\theta_e = 75°$ and $\theta_e = 90°$. In addition, Figure 10 demonstrates the effect of the substrate wettability expressed in terms of θ_e on the spreading process: the droplet on a substrate of higher wettability (i.e., smaller θ_e) is spreading faster from the very beginning. This can be rationalized by the fact that a mismatch between θ_0 and θ_e serves as a driving force for droplet spreading. Therefore, a larger difference between them leads to a faster spreading.

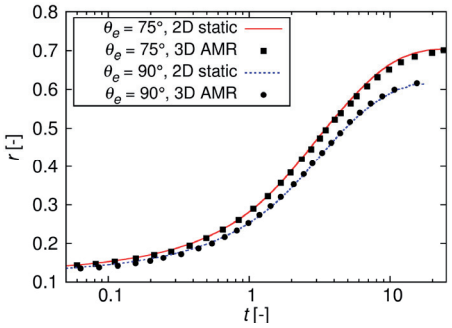

Figure 10: Temporal evolution of droplet's base radius from 2D static-mesh axisymmetric and 3D AMR simulations, $Re = 1.0$, $Ca = 0.94$, $Pe_\kappa = 1000$, $Cn = 0.01$, $Eo = 0$, $\theta_0 = 170°$, $\lambda_\mu = 0.1$.

3.2.2 Droplet wetting on inclined plane

A 3D AMR simulation of a droplet wetting on an inclined substrate is plotted in Figure 11. At first, due to the combined capillary and gravity forces, the droplet starts to spread and deforms to the inclination direction (Figure 11a and Figure 11b). Then, driven by gravity, it slides down the substrate at a constant velocity and keeps the deformed shape (Figure 11c). The contact angle hysteresis phenomenon (i.e., different advancing and receding apparent contact angles) is successfully reproduced in the simulation.

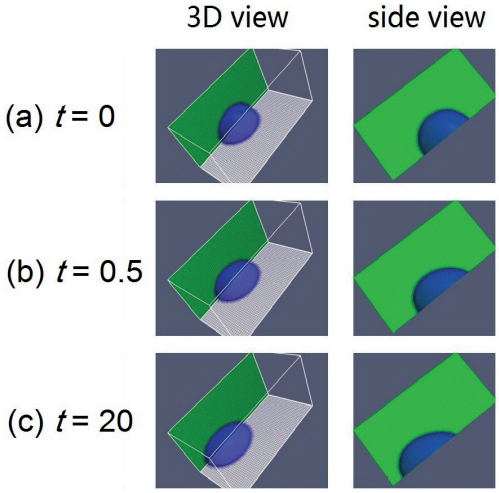

Figure 11: 3D AMR simulation of a droplet (one half geometry) on an inclined plane (inclination angle $\alpha = 45°$) from initial state (a) to constantly-sliding state (c). $\theta_0 = \theta_e = 90°$, $Re = 1.0$, $Ca = 0.94$, $Pe_\kappa = 1000$, $Cn = 0.01$, $Eo = 5$, $\lambda_\mu = 0.1$.

Figure 12 depicts the simulated temporal evolution of the position of the droplet front s, for different values of Pe_κ. Like in the previous simulation of droplet spreading on flat surface, the motion of contact line is driven by diffusion.

Therefore, the droplet is sliding down faster at a smaller Pe_κ. From the slope in Figure 12, one can compute the droplet sliding speed. Obviously, this speed depends critically on the Peclet number, respectively the mobility, which itself relates to a slip length. Thus, we have to note that the method is currently not predictive for the speed of a droplet on an inclined plane, since it is not clear a priori which value to choose for the mobility.

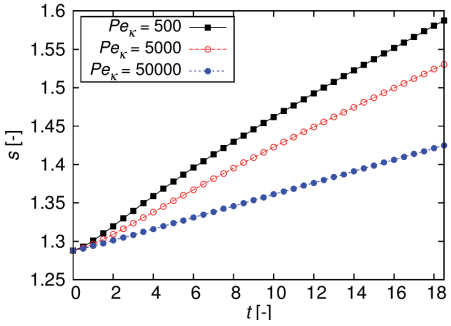

Figure 12: Instantaneous position of droplet front s. $\theta_0 = \theta_e = 90°$, $Re = 1.0$, $Ca = 1.42$, $Cn = 0.01$, $Eo = 11$, $\lambda_\mu = 1$, $\alpha = 28°$, droplet volume $V = 77.8$ mm^2.

4. Conclusions and outlook

In this paper, we have investigated wetting phenomena numerically with a phase-field method. Both, for capillary rise between parallel plates and droplet wetting on flat substrates, computed steady geometrical parameters agree well with the relevant analytical solutions. Concerning droplet spreading, the time dependent simulation results are in good agreement with experimental data of Zosel. Furthermore, the method's ability of 3D adaptive mesh refinement simulations has been demonstrated for two cases, namely droplet wetting on a flat substrate and a droplet running down an inclined plane. For the latter cases, we found that the dynamics of the simulated wetting process (motion of contact line, sliding speed of the droplet) are strongly influenced by the Peclet number Pe_κ, respectively the mobility. In diffuse interface methods, the mobility can be related to the slip length in sharp interface methods [12]. In ongoing work, we are continuing to study the effect of Pe_κ on dynamic wetting processes in order to validate the method and make it predictive.

As next steps, we are developing a volume-conservative and bounded phase field framework incorporating both Cahn-Hilliard and Allen-Cahn equations, where a relative density flux in momentum equation is introduced to guarantee volume conservation for two-phase flows with large density ratios [13]. Up to now, we have employed the wall energy formulation accounting for equilibrium contact angle alone; next, we will develop a wall energy relaxation model for dynamic contact angle. Furthermore, we will investigate wetting phenomena on chemically and geometrically heterogeneous surfaces.

Acknowledgment

We gratefully acknowledge the funding by Helmholtz Energy Alliance "Energy-efficient chemical multiphase processes" (HA-E-0004).

REFERENCES

1. Huh, C. and L.E. Scriven, Hydrodynamic Model of Steady Movement of a Solid/Liquid/Fluid Contact Line. J Colloid Interf Sci, 1971. 35(1): p. 85-101.
2. De Gennes, P.-G., Wetting: statics and dynamics. Rev Mod Phys, 1985. 57(3): p. 827.
3. Renardy, M., Y. Renardy, and J. Li, Numerical Simulation of Moving Contact Line Problems Using a Volume-of-Fluid Method. J Comput Phys, 2001. 171(1): p. 243-263.
4. Jacqmin, D., Calculation of Two-Phase Navier-Stokes Flows Using Phase-Field Modeling. J Comput Phys, 1999. 155(1): p. 96-127.
5. Waals, J.D.v.d., The thermodynamic theory of capillarity under the hypothesis of a continuous variation of density (in Dutch). Verhandel/Konink Akad Weten, 1879. 1: p. 8.
6. Anderson, D.M., G.B. McFadden, and A.A. Wheeler, Diffuse-interface methods in fluid mechanics. Ann Rev Fluid Mech, 1998. 30: p. 139-165.
7. Jacqmin, D., Contact-line dynamics of a diffuse fluid interface. J Fluid Mech, 2000. 402: p. 57-88.
8. Cai, X., M. Wörner, and O. Deutschmann, Implementation of a Phase Field Method in OpenFOAM® for Simulation of Spreading Droplets and Verification by Test Problems, in 7th Open Source CFD Int Conf. 2013: Hamburg, Germany.
9. Gennes, P.-G.d., F. Brochard-Wyart, and D. Quéré, Capillarity and wetting phenomena : drops, bubbles, pearls, waves. 2004, New York: Springer. xv, 291 p.
10. Zosel, A., Studies of the Wetting Kinetics of Liquid-Drops on Solid-Surfaces. Colloid Polym Sci, 1993. 271(7): p. 680-687.
11. Zhou, C., et al., 3D phase-field simulations of interfacial dynamics in Newtonian and viscoelastic fluids. J Comput Phys, 2010. 229(2): p. 498-511.
12. Yue, P.T., C.F. Zhou, and J.J. Feng, Sharp-interface limit of the Cahn-Hilliard model for moving contact lines. J Fluid Mech, 2010. 645: p. 279-294.
13. Abels, H., H. Garcke, and G. Grün, Thermodynamically consistent, frame indifferent diffuse interface models for incompressible two-phase flows with different densities. Math Mod Meth Appl S, 2012. 22(3).